A General Contact Force Analysis of an Under-actuated Finger in Robot Hand Grasping

Regular Paper

Xuan Vinh Ha[1], Cheolkeun Ha[1]* and Dang Khoa Nguyen[1]

1 School of Mechanical Engineering, University of Ulsan, Ulsan, Republic of Korea
*Corresponding author(s) E-mail: cheolkeun@gmail.com

Abstract

This paper develops a mathematical analysis of contact forces for the under-actuated finger in a general under-actuated robotic hand during grasping. The concept of under-actuation in robotic grasping with fewer actuators than degrees of freedom (DOF), through the use of springs and mechanical limits, allows the hand to adjust itself to an irregularly shaped object without complex control strategies and sensors. Here the main concern is the contact forces, which are important elements in grasping tasks, based on the proposed mathematical analysis of their distributions of the n-DOF under-actuated finger. The simulation results, along with the 3-DOF finger from the ADAMS model, show the effectiveness of the mathematical analysis method, while comparing them with the measured results. The system can find magnitudes of the contact forces at the contact positions between the phalanges and the object.

Keywords Under-actuated Mechanism, Robotic Gripper, Contact Forces, Grasping, Kinetostatic Analysis

1. Introduction

Several researchers have investigated different types of devices for grasping and handling unstructured objects. Such a device must adapt itself to the shape being grasped. An isotropic gripper that provides uniform contact pressure is introduced in [1], while the closest gripper to the human finger required more than ten actuators and sensors [2]. Many dexterous hands that have several actuators can be mentioned, such as the Utah/MIT hand [3], the Stanford/JPL Salisbury's hand [4], the Belgrade hand revisited at USC [5] and the DLR hand [6].

As one example of research in the robotic hand field, J.A. Corrales et al. developed the kinematic, dynamic and contact models of a three-fingered robotic hand (Barrett-Hand) in order to obtain a complete description of the system required for manipulation tasks [7]. Another study by R. Rizk et al. introduced the grasp stability of an isotropic under-actuated finger, which is made by two phalanges, and uses cams and tendon for actuation [8]. They also presented a study of the internal forces developed in the transmission chains. G. Dandash presents the design of a three-phalanx, pseudo-isotropic, under-actuated finger with anthropomorphic dimensions. Two cams were used to ensure grasping was as isotropic as possible [9]. Additionally, for a multi-fingered tele-manipulation system, Angelika Peer et al. presented a point-to-point mapping algorithm, which depends largely on the object identification process and the estimation of human intention. It allows the system to map fingertip

motions of a human hand to a three-finger robotic gripper, known as the BarrettHand [10].

The dexterity can also be obtained by under-actuation, which consists of equipping the finger with fewer actuators than the number of DOF. Thus, Thierry Laliberté et al. addressed the simulation and design of under-actuated mechanical hands to grasp a wide variety of objects with large forces in industrial tasks. Architectures of 2-DOF under-actuated fingers are proposed and their behaviour is analysed through a simulation tool. A design of a three-fingered hand is then proposed using a chosen finger [11]. The design of a 3-DOF finger is also discussed with stability of grasp, equilibrium and ejection problems in [12]. In [13], Dalibor Petkovic et al. investigate a kinetostatic model of a design for an under-actuated robotic gripper with fully distributed compliance. Given the highly non-linear system and complicated mathematical model, an approximated adaptive neuro-fuzzy inference system (ANFIS) is proposed for forecasting the gripper contact forces. Moreover, Lionel Girglen et al. analysed several common differential mechanisms modelled as basic force transmission, such as a movable pulley, seesaw mechanism, fluidic T-pipe, and planetary and bevel gear differentials. A mathematical method to obtain the output force capabilities of connected differential mechanisms is presented and two types of under-actuated robotic hands are introduced in [14]. In [15], a fundamental basis of the analysis of under-actuated fingers with a general approach is established. This method proposes two matrices that describe the relationship between the input torque of the finger actuator(s) and the contact forces on the phalanges.

Another approach, LARM Hand, which includes three fingers, was designed for anthropomorphic behaviour. Marco Ceccarelli et al. [16] proposed the grasping adaptation of a 1-DOF anthropomorphic finger mechanism in LARM Hand by using flexible links and/or under-actuated mechanisms with additional spring elements or flexural joints. For a flexible mechanism, flexible links and joints were represented through lumped spring elements, while the under-actuated mechanism was obtained by substituting a crank of the original four-bar linkage with a dyad, whose links are connected by a spring element. In addition, a new finger mechanism with an active 1-DOF was investigated to improve an existing prototype of LARM Hand with a torsional spring at a rotational joint, while a sliding joint is used for the linear spring to achieve a flexible link [17]. The proposed mechanism is not simple since it is composed of seven links, one slider and two springs. In addition, it is requested to be sized within a finger body with human-like size and to operate with an anthropomorphic grasp behaviour.

The introduction of two new matrices in [15] allows the system to calculate the contact forces on the phalanges through the input torque of the finger actuator in the case of full-phalanx grasping. However, in the case of fewer-than-n phalanx grasping, it is difficult to obtain the contact forces based on the relationship between the input torque of the finger actuator and the contact forces on phalanges. This paper proposes a general mathematical analysis of the distributions of contact forces for the under-actuated finger in the case of full-phalanx grasping, while taking into account cases of fewer-than-n phalanx grasping. The simulation results, with the 3-DOF finger model from the ADAMS environment, show the effectiveness of the mathematical analysis method, while comparing with the measured results. The system can find magnitudes of the contact forces at the contact positions between the finger phalanges with the object.

The remainder of this paper is organized in eight sections. The related works are introduced in Section 2. Section 3 reviews the original analysis of an n-DOF under-actuated finger. Section 4 proposes the general contact force analysis of an under-actuated finger. Simulation set-up is introduced in Section 5. Section 6 shows the simulation results. Discussion is mentioned in Section 7. Finally, Section 8 presents the conclusions.

2. Related works

Contact forces play an important role in grasping tasks of the Robot Hand. Contact forces depend mainly on the actuator torque and the torque transmission ratio between under-actuated joints. R. Rizk et al. analysed the contact forces of the under-actuated finger, which is made by two phalanges and uses cams and tendon for actuation. It allows authors to determine the grasp stability of the finger and the efforts exerted on the passive elements, respectively [8]. In [9], G. Dandash presents a method to compute the contact forces in a pulley-tendon finger. It is a matter of establishing a balance between the powers at equilibrium. In another study, Dalibor Petkovic et al. proposed an approximated ANFIS for forecasting the gripper contact forces of the under-actuated robotic gripper with fully distributed compliance because of the highly non-linear system and complicated mathematical model [13].

Several researchers have applied the mathematical analysis to calculate the contact forces in designing the gripper systems. A mathematical analysis to obtain the contact force of the under-actuated gripper was considered in [14]. In [15], the authors propose two matrices that describe the relationship between the input torque of the finger actuator(s) and the contact forces on the phalanges. In addition, Wu LiCheng et al. proposed a static analysis method to obtain the contact forces and a Jacobian matrix of the proposed finger mechanism with an active 1-DOF to improve the existing prototype of LARM Hand [17]. In another approach, the numerical simulation in ADAMS' environment is used to characterize the functionality of the new prototype, which is a new under-actuated finger mechanism for LARM hand [18].

Recently, the sensor technique has been widely developed and applied in the robotic field. Tactile sensors are devices

providing pressure data and often surficial distribution of the latter on the sensors; i.e., localization. In [19], the sensor feedbacks from force/torque sensors and tactile sensors were used to implement and validate the robust grasp primitive for a three-finger BarrettHand. In another study, Lionel Birglen et al. implemented the tactile sensors on the MARS prototype finger's phalanges to control under-actuated hands, as shown in Figure 1. The behaviour of under-actuated fingers can be substantially enhanced with tactile information [20].
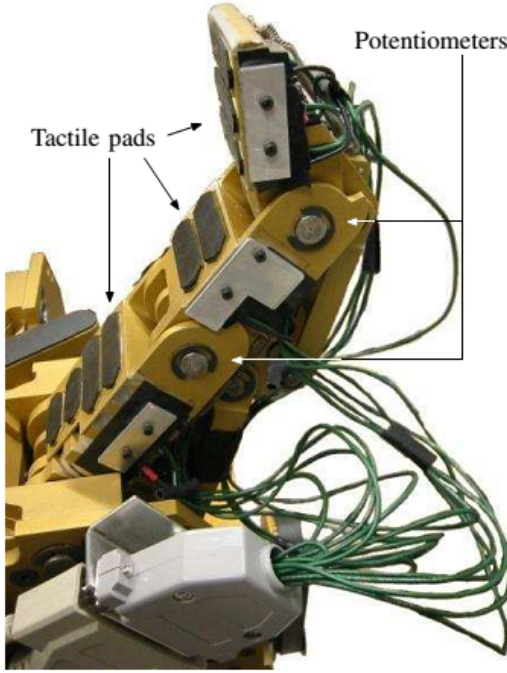
Figure 1. MARS' finger equipped with tactile sensors

3. Review of the original analysis of an under-actuated finger

3.1 General n-DOF, one degree of actuation (DOA) finger

Figure 2 illustrates the type of under-actuated n-phalanx finger considered in this section and all important parameters. The actuation wrench T_1 is applied to the input of the finger and transmitted to the phalanges through suitable mechanical elements, such as four-bar linkages. A simple kinetostatic model for the fully adaptive finger with compliant joints can be obtained by adding springs to every joint of the finger. The torque spring T_{si} in the joint O_i is used to keep the finger from incoherent motions. Passive elements are used to kinematically constrain the finger and ensure the finger adapts to the shape of the object being grasped. A grasp state is defined as the set of the geometric configurations of the finger and the contact locations on the phalanges, which are necessary to characterize the behaviour of the finger. Important parameters are denoted as follows:

L_i = the length of the ith phalanx

a_i = the length of the first driving bar of the ith four-bar linkages

b_i = the length of the ith under-actuation bar

c_i = the length of the second driving bar of the ith four-bar linkages

θ_i = the rotating angle of the ith phalanx with respect to the base

θ_{ia} = the rotating angle of the first driving bar of the ith four-bar linkages with respect to the base

ψ_i = the angle between $O_iP_i^{'}$ and O_iP_i

T_1 = the torque of the actuator at the first joint

T_{si}, $i>1$ = the spring torque of the ith joint

F_i = the contact force on the ith phalanx

k_i = the contact position on the ith phalanx

In previous research [15], Lionel Birglen et al. analysed and discussed the stability of the grasp – i.e., equilibrium and ejection phenomenon, achieving stable grasps and phalanx force distribution, and avoiding weak last phalanges that cannot ensure sufficient force to secure the grasp.
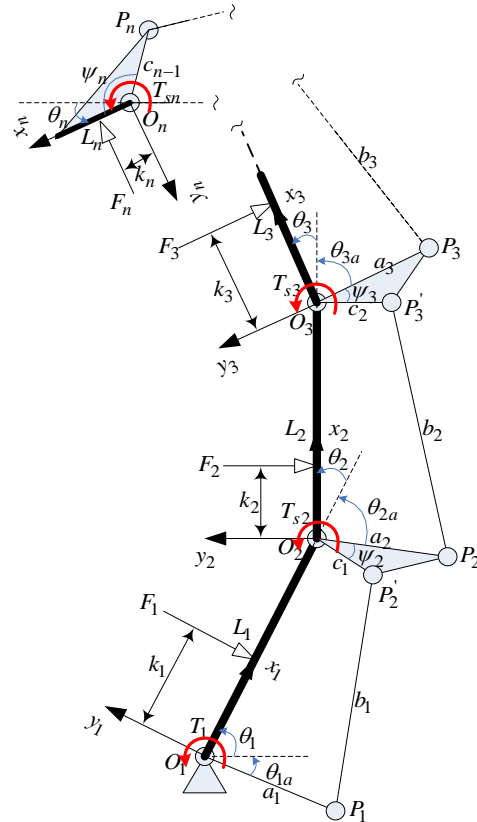

Figure 2. Geometric and force parameters of under-actuated n-DOF finger

3.2 Static analysis of under-actuated n-DOF finger

Even though three phalanges are normally used for robot fingers, this section considers a general n-DOF, 1-DOA finger with four-bar linkages for general static analysis. The finger model is illustrated in Figure 2.

To determine the distributions of the contact forces that depend on the contact point location and the joint torques inserted by springs, we proceed with a static modelling of the finger. Additionally, the friction must be ignored and the grasping object has to be fixed. Equating the input and the output virtual powers of the finger [15] yields:

$$T^T \omega_a = F^T v \tag{1}$$

where T is the input torque vector by the actuator and springs, ω_a is the corresponding velocity vector, F is the contact force vector, and v is the projected velocity vector of the contact points; i.e.,

$$T = \begin{bmatrix} T_1 \\ T_{s2} = -K_2 \Delta \theta_2 \\ T_{s3} = -K_3 \Delta \theta_3 \\ \dots \\ T_{sn} = -K_n \Delta \theta_n \end{bmatrix}, \omega_a = \begin{bmatrix} \dot{\theta}_{1a} \\ \dot{\theta}_{2a} \\ \dot{\theta}_{3a} \\ \dots \\ \dot{\theta}_n \end{bmatrix}, F = \begin{bmatrix} F_1 \\ F_2 \\ F_3 \\ \dots \\ F_n \end{bmatrix} and \ v = \begin{bmatrix} v_{yc1} \\ v_{yc2} \\ v_{yc3} \\ \dots \\ v_{ycn} \end{bmatrix} \tag{2}$$

where K_i is the stiffness of the torsional spring located at joint O_i, and Δ_i, $i > 1$ is the difference between the current and initial angles of the joint O_i.

Thus, the projected velocities can be simply expressed as a product of a Jacobian matrix J_T and the derivative vector of the phalanx joint coordinates $\theta = [\theta_1, \theta_2, \theta_3, ..., \theta_n]^T$; i.e.,

$$v = J_T \dot{\theta} \tag{3}$$

As illustrated in Figure 2, the Jacobian matrix J_T of the projected velocities can be obtained in a lower triangular form:

$$J_T = \begin{bmatrix} k_1 & 0 & 0 & \dots & 0 \\ \alpha_{12} & k_2 & 0 & \dots & 0 \\ \alpha_{13} & \alpha_{23} & k_3 & \dots & 0 \\ \dots & \dots & \dots & \dots & \dots \\ \alpha_{1n} & \alpha_{2n} & \alpha_{3n} & \dots & k_n \end{bmatrix} \tag{4}$$

where

$$\alpha_{ii} = k_i \tag{5}$$

and

$$\alpha_{ij} = k_j + \sum_{k=i}^{j-1} L_k \cos\left(\sum_{m=k+1}^{j} \theta_m\right), \qquad i < j \tag{6}$$

Through differential calculus, one can also relate the vector to the derivatives of the phalanx joint coordinates defined previously with an actuation Jacobian matrix J_a :

$$\dot{\theta} = J_a \omega_a \tag{7}$$

In the under-actuated finger model, the four-bar linkage is used to transmit the actuator torque to each phalanx, while the principle of transmission gives the angular velocity ratio of four-bar linkage, known as Kennedy's Theorem [21-22]. With the ith four-bar linkage $O_i P_i P'_{i+1} O_{i+1}$, we have:

$$\dot{\theta}_i = \dot{\theta}_{ia} + \dot{\theta}_{i+1a} \frac{c_i \left(L_i \sin(\theta_{i+1a} - \psi_{i+1}) - a_i \sin(\theta_i - \theta_{ia} + \theta_{i+1a} - \psi_{i+1}) \right)}{a_i \left(L_i \sin(\theta_i - \theta_{ia}) + c_i \sin(\theta_i - \theta_{ia} + \theta_{i+1a} - \psi_{i+1}) \right)} \tag{8}$$

From the last four-bar linkage, $O_{n-1} P_{n-1} P_n O_n$, we have:

$$\dot{\theta}_{n-1} = \dot{\theta}_{n-1a} + \dot{\theta}_n \frac{c_{n-1} \left(L_{n-1} \sin(\theta_n - \psi_n) - a_{n-1} \sin(\theta_{n-1} - \theta_{n-1a} + \theta_n - \psi_n) \right)}{a_{n-1} \left(L_{n-1} \sin(\theta_{n-1} - \theta_{n-1a}) + c_{n-1} \sin(\theta_{n-1} - \theta_{n-1a} + \theta_n - \psi_n) \right)} \tag{9}$$

From Equations (8) and (9), Equation (7) can be described by Equation (10) as:

$$\begin{bmatrix} \dot{\theta}_1 \\ \dot{\theta}_2 \\ \dot{\theta}_3 \\ \dots \\ \dot{\theta}_n \end{bmatrix} = \begin{bmatrix} 1 & X_1 & 0 & \dots & 0 \\ 0 & 1 & X_2 & \dots & 0 \\ \dots & \dots & \dots & \dots & \dots \\ 0 & 0 & 0 & \dots & X_{n-1} \\ 0 & 0 & 0 & \dots & 1 \end{bmatrix} \begin{bmatrix} \dot{\theta}_{1a} \\ \dot{\theta}_{2a} \\ \dot{\theta}_{3a} \\ \dots \\ \dot{\theta}_n \end{bmatrix}, or \quad \dot{\theta} = J_a \omega_a \tag{10}$$

where

$$J_a = \begin{bmatrix} 1 & X_1 & 0 & \dots & 0 \\ 0 & 1 & X_2 & \dots & 0 \\ \dots & \dots & \dots & \dots & \dots \\ 0 & 0 & 0 & \dots & X_{n-1} \\ 0 & 0 & 0 & \dots & 1 \end{bmatrix} \tag{11}$$

$$X_i = \frac{c_i \left(L_i \sin(\theta_{i+1a} - \psi_{i+1}) - a_i \sin(\theta_i - \theta_{ia} + \theta_{i+1a} - \psi_{i+1}) \right)}{a_i \left(L_i \sin(\theta_i - \theta_{ia}) + c_i \sin(\theta_i - \theta_{ia} + \theta_{i+1a} - \psi_{i+1}) \right)} \tag{12}$$

$$X_{n-1} = \frac{c_{n-1} \left(L_{n-1} \sin(\theta_n - \psi_n) - a_{n-1} \sin(\theta_{n-1} - \theta_{n-1a} + \theta_n - \psi_n) \right)}{a_{n-1} \left(L_{n-1} \sin(\theta_{n-1} - \theta_{n-1a}) + c_{n-1} \sin(\theta_{n-1} - \theta_{n-1a} + \theta_n - \psi_n) \right)} \tag{13}$$

and X_i is a function that is used to transmit the actuator torque to the ith phalanx. Finally, from Equations (1), (3) and (7), we obtain:

$$F = J_T^{-T} J_a^{-T} T \tag{14}$$

which is the equation that provides a practical relationship between the actuator torques and contact forces. Equation (14) is valid if and only if $k_1k_2k_3...k_n \neq 0$, which is the condition of singularity for the J_T matrix. J_a cannot be singular; however, the finger may contact the object in the case that fewer-than-n phalanges are touching the object. That assumption leads to the singularity of the J_T matrix, such that Equation (14) cannot perform.

3.3 Stability of the grasp of the 3-DOF under-actuated finger

We will now analyse the stability of the grasp of the under-actuated 3-DOF finger. The geometric and force parameters under-actuated 3-DOF finger are described in Figure 3, while its real structure design is shown in Figure 4. The identified parameters of the finger are illustrated on Table 1.
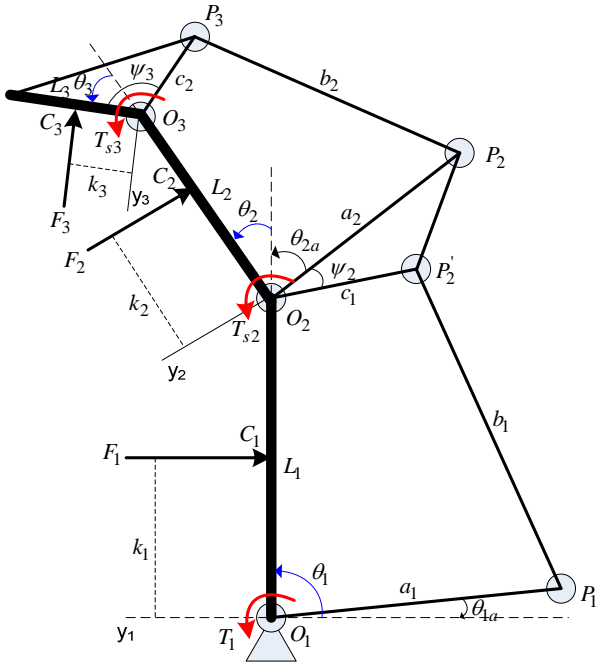
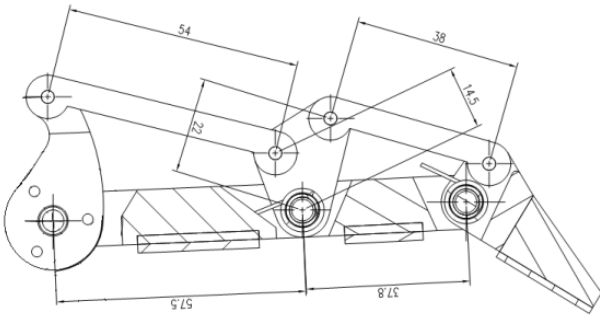**Figure 3.** Geometric and force parameters of under-actuated 3-DOF finger

Figure 4. The structure design of the under-actuated finger

Firstly, the behaviour of the finger is largely determined by its geometry, prescribed at the design stage. Depending on

a_1 [mm]	28.5	a_2 [mm]	22.0
b_1 [mm]	54.0	b_2 [mm]	38.0
c_1 [mm]	14.5	c_2 [mm]	10.0
L_1 [mm]	57.5	ψ_2 [degree]	42.5
L_2 [mm]	37.8	ψ_3 [degree]	90.0
L_3 [mm]	34.5		

Table 1. The identified parameters of the 3-DOF finger

the geometric parameters of the mechanism, one can obtain the final stability of the grasp. Hence, the choice of the design parameters is a very important issue when obtaining stable grasps and a proper distribution of the forces among the phalanges.

The parameters, illustrated in Figure 3, will now be discussed. The length of the phalanges - i.e., L_1, L_2 and L_3 - are fixed from comparison with other existing fingers, simulations and experimentation with a finger model on objects to be grasped. The remaining parameters are a_i, b_i, c_i and ψ_i. In order to reduce the number of independent variables, some relationships between these parameters are imposed, while the number of variables is reduced to two. It was clearly shown that the behaviour of the fingers is mainly dictated by the ratios $R_i = a_i / c_i$, $i = 1, 2$ [11]. In [12], Thiery Lalibeté et al. referred to the global performance index to evaluate the criteria that was used to determine the performance of the fingers. The graph of the global performance index was a function of R_1 and R_2. An effective finger, including the stable grasps, could then be chosen among the best values. From our finger design, R_1 and R_2 are approximately 2 and 2.2, respectively (which correspond approximately to the R_1 and R_2 in [12]).

Secondly, the mechanical limit allows a pre-loading of the spring to prevent any undesirable motion of the second and third phalanges due to its own weight and/or inertial effects, as well as to prevent hyperflexion of the finger.

The set of the contact situations pair (k, θ) corresponds to the stable part of the space; namely, the space of contact configurations, where $k = [k_1, k_2, k_3]^T$ and $\theta = [\theta_1, \theta_2, \theta_3]^T$. A contact situation pair, which affects a stable grasp, corresponds to a vector F where no component is negative. If springs are neglected, expressions of the latter vectors become most simple. θ_1 is obviously absent from the expressions because rotation about this axis leaves the mechanism in the same kinematic configuration (the finger is rotated as one single rigid body). It can also be shown that signs of elements are independent of k_1; the proof is, however, more cumbersome and relies on the general inverse calculus by means of co-factors [15].

Coming back to our issue, the set of parameters presented in Table 1 (which corresponds approximately to the parameters used in prototypes of under-actuated hands [15]), taking into account the mechanical joint limits, $0 < \theta_2 < 90^o$, $0 < \theta_3 < 90^o$ and $0 < k_i < L_i$, $i = 2, 3$, the volume of the stable three-phalanx grasps is approximately 32% of the

whole space of contact configurations. Similarly, the design presented in [11] insists on the mechanical joint limits of $0<\theta_i<90^o$ to avoid the latter type of ejection. Furthermore, one should remember that full-phalanx grasps correspond only to a part of the whole possible grasps. That is, fewer-than-full phalanx grasps can also be stable [15]. Mechanical limits are key elements in the design of under-actuated fingers when considering stability issues, because they limit the shape adaptation to reasonable configurations (thus avoiding ejection).

4. The general contact force analysis of under-actuated finger

4.1 Case of n-DOF, 1-DOA finger

According to Lionel Birglen et al. [15], in order for a less-than-n phalanx grasp to be stable, every phalanx in contact with the object should have a strictly positive corresponding force. Actually, the contacts appear not only with all phalanges, but also with fewer-than-n phalanges in object grasping. The corresponding generated forces for phalanges not in contact with the object should be zero, since the latter forces can also be seen as the external forces needed to counter the actuation torque. However, calculating contact forces in the case of fewer-than-n phalanges touching the object by using Equation (14) can be a problem because of the singularity of the J_T matrix. This section tries to solve that problem by proposing a general method to determine the distributions of contact forces in all cases of gripper behaviours in object grasping. In order to do that, we assume that the stability of the grasp must be satisfied in all cases.

From Equations (1), (3) and (7), we also obtain:

$$J_T^T F = J_a^{-T} T \tag{15}$$

From Equation (15), the component $J_a^{-T} T$ on the right side is the torque vector $\tau = [\tau_1, \tau_2, ... \tau_n]^T$ at all joints of the finger (where τ_i is the torque at the ith joint) relating to the actuator, spring torques and functions of torque transmission between actuation and phalanges, as follows:

$$
\begin{bmatrix} \tau_1 \\ \tau_2 \\ \tau_3 \\ ... \\ \tau_n \end{bmatrix} = J_a^{-T} T =
\begin{bmatrix} 1 & X_1 & 0 & ... & 0 \\ 0 & 1 & X_2 & ... & 0 \\ ... & ... & ... & ... & ... \\ 0 & 0 & 0 & ... & X_{n-1} \\ 0 & 0 & 0 & ... & 1 \end{bmatrix}^{-T}
\begin{bmatrix} T_1 \\ T_{s2} \\ T_{s3} \\ ... \\ T_{sn} \end{bmatrix}
$$

$$
= \begin{bmatrix} T_1 \\ T_{s2} - X_1 T_1 \\ T_{s3} - X_2 T_{s2} + X_1 X_2 T_1 \\ ... \\ T_{sn} + \sum_{j=1}^{n-1} \left[(-1)^{n-j} \prod_{i=j}^{n-1} X_i T_{si} \right] \end{bmatrix}, \quad T_{s1} \equiv T_1 \tag{16}
$$

The left component in Equation (15) can be expressed as:

$$
J_T^T F =
\begin{bmatrix} k_1 & 0 & 0 & ... & 0 \\ \alpha_{12} & k_2 & 0 & ... & 0 \\ \alpha_{13} & \alpha_{23} & k_3 & ... & 0 \\ ... & ... & ... & ... & ... \\ \alpha_{1n} & \alpha_{2n} & \alpha_{3n} & ... & k_n \end{bmatrix}^T
\begin{bmatrix} F_1 \\ F_2 \\ F_3 \\ ... \\ F_n \end{bmatrix} \tag{17}
$$

From Equations (16-17), the general Equation (15) then becomes Equation (18):

$$
\begin{bmatrix} k_1 & 0 & 0 & ... & 0 \\ \alpha_{12} & k_2 & 0 & ... & 0 \\ \alpha_{13} & \alpha_{23} & k_3 & ... & 0 \\ ... & ... & ... & ... & ... \\ \alpha_{1n} & \alpha_{2n} & \alpha_{3n} & ... & k_n \end{bmatrix}^T
\begin{bmatrix} F_1 \\ F_2 \\ F_3 \\ ... \\ F_n \end{bmatrix} =
\begin{bmatrix} \tau_1 \\ \tau_2 \\ \tau_3 \\ ... \\ \tau_n \end{bmatrix} \tag{18}
$$

Equation (18) shows that the torque τ_i at the ith joint of the finger is calculated with respect to the contact forces vector F and parameters α_{ij} in Equation (19):

$$\sum_{j=i}^{n} \alpha_{ij} F_j = \tau_i, \quad \alpha_{ii} = k_i \tag{19}$$

In the case of fewer-than-n phalanges touching the object (e.g., when the ith phalanx is not touching the object), the parameters α_{ij} in Equation (19) are not relevant and F_i is zero. As this means that Equation (19) is not suitable for this condition, we do not need to consider this equation to compute the torque τ_i in the case of the ith phalanx not touching the object. As mentioned above, in order to calculate the contact forces vector F in Equation (18), except for F_i, we use the following process:

- Neglect the ith column in the matrix J_T because all parameters α_{ij}, $j=1...n$ do not exist.

- Neglect the ith row in the matrix J_T because all parameters α_{ji}, $j=1...n$ relate to $F_i=0$ on the left side.

- Remove the $F_i=0$ element of the force vector F on the left side.

- Neglect the τ_i element at the ith joint of the torque vector τ on the right side.

After neglecting the ith column and i^{th} row, the J_T matrix dimension is reduced by $n-1 \times n-1$, while J_T is guaranteed not to be singular. Consequently, Equation (18) can be used to calculate the contact forces, except for F_i. The above process is also used in the case of more than one phalanx not touching the object.

4.2 The case of 3-DOF, 1-degree-of actuation finger

In case of the under-actuated 3-DOF, Equation (14) is valid if and only if $k_1 k_2 k_3 \neq 0$, which is the condition of singularity for the J_T matrix, as shown in Figure 5a. However, the

finger can contact the object in the case of one or two phalanges of the finger not touching the object, as shown in Figures 5b, 5c and 5d.

In order to calculate the contact forces, F_1, F_2 and F_3, in the grasping object, we must separate the behaviours between the finger and object into four cases:
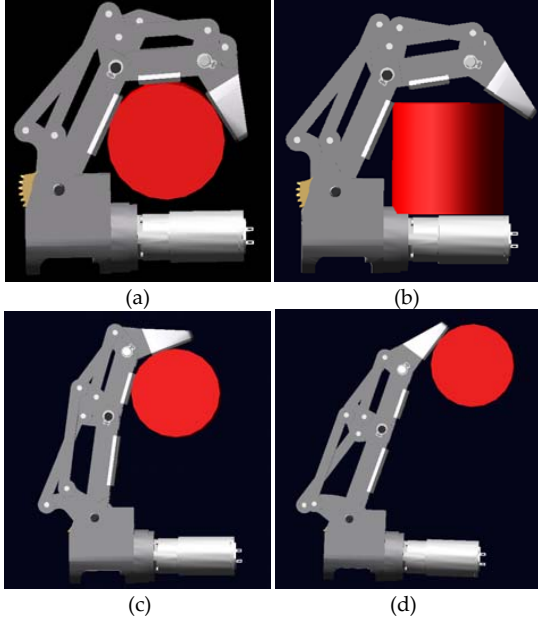

Figure 5. Four cases of finger grasping

Case 1: All three phalanges of the finger contact the object, which means that $k_1 k_2 k_3 \neq 0$, as shown in Figure 5a. From Equation (18), we then derive a practical relationship between the actuator torques and contact forces by Equation (20).

$$
\begin{bmatrix} k_1 & k_2 + L_1 C_2 & k_3 + L_1 C_{23} + L_2 C_3 \\ 0 & k_2 & k_3 + L_2 C_3 \\ 0 & 0 & k_3 \end{bmatrix} \begin{bmatrix} F_1 \\ F_2 \\ F_3 \end{bmatrix}
$$
$$
= \begin{bmatrix} T_1 \\ T_{s2} - X_1 T_1 \\ T_{s3} - X_2 T_{s2} + X_1 X_2 T_1 \end{bmatrix} \tag{20}
$$

From Equation (20), the three contact forces, F_1, F_2 and F_3, are computed by using Equations (21), (22) and (23), respectively.

$$
F_1 = \frac{T_1}{k_1} - \frac{(k_2 + L_1 C_2)(T_{s2} - X_1 T_1)}{k_1 k_2}
$$
$$
- \frac{(k_3 + L_1 C_{23} + L_2 C_3)(T_{s3} - X_2 T_{s2} + X_1 X_2 T_1)}{k_1 k_3} \tag{21}
$$
$$
+ \frac{(k_2 + L_1 C_2)(k_3 + L_2 C_3)(T_{s3} - X_2 T_{s2} + X_1 X_2 T_1)}{k_1 k_2 k_3}
$$

$$
F_2 = \frac{T_{s2} - X_1 T_1}{k_2} - \frac{(k_3 + L_2 C_3)(T_{s3} - X_2 T_{s2} + X_1 X_2 T_1)}{k_2 k_3} \tag{22}
$$

$$
F_3 = \frac{T_{s3} - X_2 T_{s2} + X_1 X_2 T_1}{k_3} \tag{23}
$$

Case 2: The proximal and distal phalanges contact with the object, which means the parameter k_2 does not exist, while F_2 is zero, as illustrated in Figure 5b. From Equation (20), the second column and row in the J_T matrix relating to the medial phalanx are removed, as well as the elements F_2 and $\tau_2 = T_{s2} - X_1 T_1$ in the F and τ vectors. Equation (20) then becomes:

$$
\begin{bmatrix} k_1 & k_3 + L_1 C_{23} + L_2 C_3 \\ 0 & k_3 \end{bmatrix} \begin{bmatrix} F_1 \\ F_3 \end{bmatrix} = \begin{bmatrix} T_1 \\ T_{s3} - X_2 T_{s2} + X_1 X_2 T_1 \end{bmatrix} \tag{24}
$$

with F_1 and F_3 then calculated using Equations (25) and (23), respectively.

$$
F_1 = \frac{T_1}{k_1} - \frac{(k_3 + L_1 C_{23} + L_2 C_3)(T_{s3} - X_2 T_{s2} + X_1 X_2 T_1)}{k_1 k_3} \tag{25}
$$

Case 3: The medial and distal phalanges contact the object, meaning that the parameter k_1 does not exist and F_1 is zero, as shown in Figure 5c. From Equation (20), the first column and row in the J_T matrix relating to the proximal phalanx are removed, as well as the elements F_1 and τ_1 in the F and τ vectors. Equation (20) then becomes:

$$
\begin{bmatrix} k_2 & k_3 + L_2 C_3 \\ 0 & k_3 \end{bmatrix} \begin{bmatrix} F_2 \\ F_3 \end{bmatrix} = \begin{bmatrix} T_{s2} - X_1 T_1 \\ T_{s3} - X_2 T_{s2} + X_1 X_2 T_1 \end{bmatrix} \tag{26}
$$

F_2 and F_3 are calculated by using Equations (22) and (23), respectively.

Case 4: Finally, the distal phalanx contacts the object, which means the parameters k_1 and k_2 do not exist, while F_1 and F_2 are zero, as shown in Figure 5d. From Equation (20), the first and second column and row in the J_T matrix relating to the proximal and medial phalanges are removed, as well as the elements F_1, F_2, τ_1 and τ_2 in the F and τ vectors. Equation (20) then becomes:

$$
k_3 F_3 = T_{s3} - X_2 T_{s2} + X_1 X_2 T_1 \tag{27}
$$

F_3 is calculated by using Equation (23).

5. Set-up

5.1 Gripper model set-up

Since the complexity of products has been increasing, in order to increase competition in production, the require-

ment of the product development cycle times ought to be reduced. Therefore, building a hardware prototype for testing has taken the majority of time for launching new product. The simulation technique based on the virtual prototype is proposed as an approach that significantly reduces manufacturing cost and time, compared to the traditional build-and-test approach. The virtual prototyping approach is an integrating software solution that consists of modelling a mechanical system, simulating and visualizing its 3D motion behaviour under real world operating conditions, and refining and optimizing the design through iterative design studies. The advantages of this simulation technique consist of conceiving a detailed model that is used in a virtual experiment similar to one in a real scenario. Virtual measurements of parameters and components of the mechanical model can also be carried out conveniently. Figure 6 shows the creation of a virtual prototype for testing and simulating the gripper system. The Computer- Aided Design (CAD) drawing of the adaptive gripper was designed by a company in the Republic of Korea.

Figure 6. Block diagram of ADAM gripper model creation using the Matlab/Simulink Environment

The virtual prototyping platform includes software tools, such as CAD (SOLIDWORKS, CATIA, PROENGINEER), MSC ADAMS and MATLAB/Simulink. The CAD software is used to create the geometric model of the gripper mechanical system. This model includes the rigid parts with the shape and dimension of the physical prototype model, as well as containing information about mass and inertia properties of these rigid parts. The CAD geometry model is then exported to the ADAM/View environment using a file format, such as *Step* (CATIA) or *Parasolid.x_t*

(SOLIDWORKS). The ADAM/View is the tool of the virtual platform, which is used for analysing, optimising and simulating the kinematic and dynamic behaviour of the mechanical system under real operating conditions.

Normal Force: IMPACT Function model	
Stiffness	$1.0*10^8$ [N/m]
Force Exponent	1.5
Damping	$1.0*10^4$ [N/m]
Penetration Depth	$1.0*10^{-8}$ [N/m]
Friction Force: Coulomb friction	
Static Coefficient	0.7
Dynamic Coefficient	0.5
Stiction Transition Velocity	0.1 [m/s]
Friction Transition Velocity	1.0 [m/s]

Table 2. The identified contact parameters in the ADAMS model

Constructing a control system for the virtual gripper model is necessary for co-simulation of the two separate simulation programs into a whole system. The control design is developed based on ADAMS/Control and MATLAB/Simulink. To export the virtual mechanical model of the gripper from ADAMS to the MATLAB environment, the input and output variables are firstly defined in the ADAMS model. The input signals are the forces that control the servomotors of gripper fingers. Meanwhile, the output signals are the measured parameters of gear angle, screw speed, joint angles and contact forces. Subsequently, this model is exported to MATLAB/Simulink. In the MATLAB environment, a.*mfile* and an *adams_sys* are created. The *adams_sys* presents the non-linear MSC/ADAMS model with inputs and outputs. In this paper, the ADAMS finger model has a torque input and, 10 outputs, as shown in Figure 7. The ADAMS block is created based on the information from the.*mfile*.

The material types of all finger elements and the object, shown in Figure 5, are declared by dry aluminium. Then,
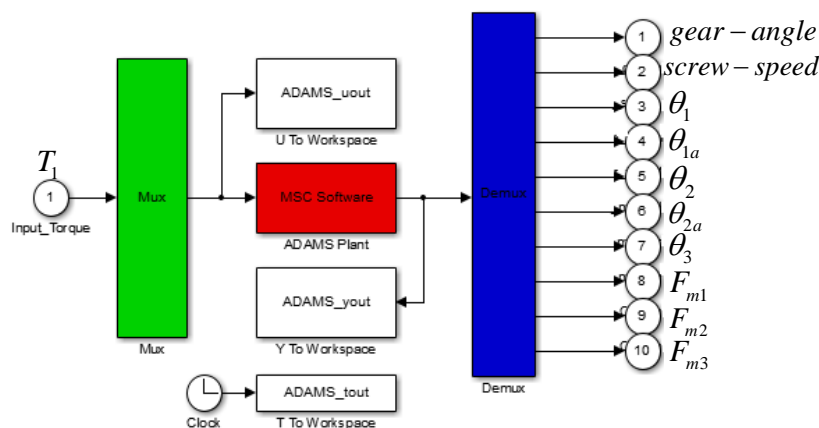

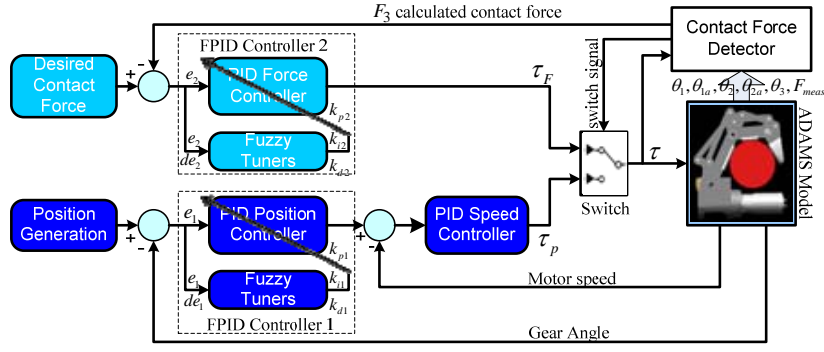**Figure 7.** The ADAM block of finger in *adams_sys*

Figure 8. The diagram of the simulated control system for one finger

the contact feature parameters between phalanges and object are chosen suitably according to the material types under real world operating conditions. Table 2 shows identified contact feature parameters at which the ADAMS contact behaviour resembles the real world contact behaviour.

5.2 The simulated control system

Since properly designed under-actuated mechanisms perform shape adaptation "automatically", no motor coordination is needed. Before performing a grasp, the geometry of the object should be determined and the hand should adjust itself to this geometry by orienting the fingers. To orient the fingers, a simple trajectory is generated to a prescribed position and the gear motor follows this trajectory with a PD/PID position control. In order to set the grasping force on the object, a maximum motor torque is set to a desired value. The relationship between the force on the object and the torque of the motor is obtained using the proposed method to determine contact forces.

In the finger control approach, an integration of position and force control methods for one finger is applied. Figure 8 shows a diagram of the simulated control system. As shown in this figure, the position control system for the finger includes two closed-loop controls: a low-level closed-loop control for motor speed (screw speed) and a high-level closed-loop control for the finger's position angle (gear angle) based on measured motor speed and gear angle feedbacks. For the low-level closed-loop control, the PID controller is applied. Meanwhile, the tuning fuzzy PID (FPID) Controller 1 is designed for high-level closed-loop control because of the non-linear system.

For the force control system, the tuning FPID Controller 2 is also used, based on the calculated contact force feedback from the Contact Force Detector (CFD) block, where the proposed method to determine contact forces in Section 4 is applied as shown in Figure 8. The inputs of the CFD block are rotating angles of phalanges and driving bars, as well as the measured contact forces and motor torque, while the outputs are three calculated contact forces on three pha-

langes. As described in Section 4, the distal phalanx of the finger always contacts the object in four cases of finger grasping. Therefore, the contact force on the distal phalanx (F_3) is chosen to control for the force control system in four cases.

In finger control strategy, there are two control processes. The first control process is used for the position angle of finger. The torque input of the ADAMS model (τ) is provided by the torque output (τ_p) of this process. This process, which controls the finger position to follow the desired position, is going to be stopped when the distal phalanx starts to touch the object in finger grasping. At that time, the CFD will issue a switch signal to control the Switch block to switch to the second process (force control process). In the second process, the FPID Controller 2 will control the distal finger touching the object based on the desired contact force.
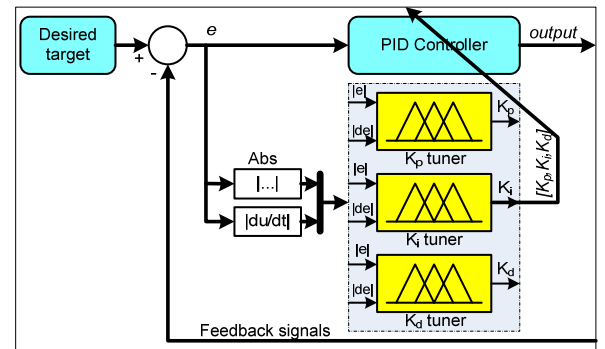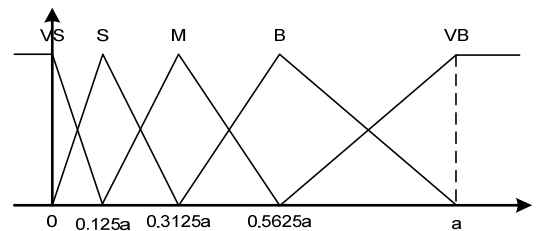

Figure 9. The tuning FPID diagram

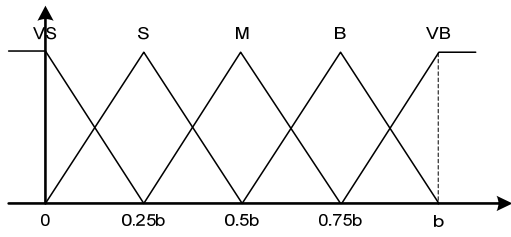**Figure 10.** Membership functions of inputs $|e|$

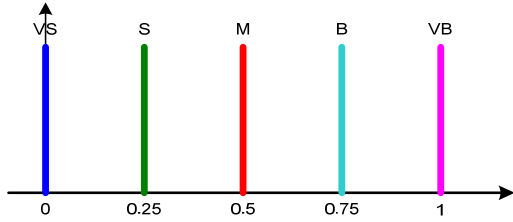**Figure 11.** Membership functions of inputs $|de|$

Figure 12. Membership functions of the outputs k_p, k_i and k_d

The detailed FPID controller is shown in Figure 9. From this figure, it can be seen that there are three fuzzy tuners for the three output parameters: K_p, K_d and K_i. Two input signals are needed for each fuzzy tuner [23]; namely, the absolute error $|e|$ and derivative error $|de|$. Triangle and trapeze membership functions are then utilized to create the fuzzy input partitions. Here, five membership functions (VS, S, M, B and B) representing the five input states (very small, small, medium, big and very big), respectively, are used for the controller. Details of the fuzzy inputs' membership functions are shown in Figures 10 and 11 (a and b parameters are two constants that are determined in experiment simulation).

There are three outputs from the three fuzzy tuners, k_p, k_i and k_d, with the outputs having ranges from 0 to 1. Singleton membership functions are then used for the fuzzy output partitions. Figure 12 shows five membership functions (VS, S, M, B and VB) corresponding with the five output states (very small, small, medium, big and very big), respectively.

k_p, k_i, k_d			$|de|$		
		VS	**S**	**M**	**B**	**VB**
	VS	VS/VS/VS	VS/VS/VS	VS/S/VS	VS/S/VS	VS/S/VS
	S	M/VS/S	M/S/S	S/S/VS	S/M/VS	S/M/VS
$|e|$	**M**	B/S/M	B/M/M	M/M/S	M/B/S	M/B/VS
	B	VB/M/B	VB/B/B	M/B/M	M/VB/M	M/VB/S
	VB	VB/VB/VB	VB/VB/VB	VB/VB/B	VB/VB/B	VB/VB/B

Table 3. Rule table of the fuzzy tuners

The design rules of the fuzzy tuners are shown in Table 3. The MAX-PROD formula is chosen as the main strategy for the implication process:

$$\mu_{out}^i = \max\left(\mu(e)\cdot\mu(de)\right) \qquad (28)$$

where $\mu(e)$ and $\mu(de)$ are membership values with respect to input variables, while μ_{out}^i is the membership value with respect to the output variable at the ith rule. The centroid de-fuzzification method is used to convert the aggregated fuzzy, which is set to a crisp output value. In this case, because the membership functions for the fuzzy output partitions are in Singleton form, the outputs of fuzzy tuners are calculated as:

$$y_{out} = \frac{\sum_{i=1}^{25} \mu_{out}^i \cdot y_{out}^i}{\sum_{i=1}^{25} \mu_{out}^i} \qquad (29)$$

where y_{out}^i is the output value of the ith rules, which can be determined in Figure 12, while the output of the fuzzy tuner y_{out} is k_p, k_i or k_d. These output values of the fuzzy tuners are then substituted into Equation (30) to compute three parameters, K_p, K_i and K_d, as follows:

$$
\begin{aligned}
K_p &= K_{p\min} + k_p(K_{p\max} - K_{p\min}) \\
K_i &= K_{i\min} + k_i(K_{i\max} - K_{i\min}) \\
K_d &= K_{d\min} + k_d(K_{d\max} - K_{d\min})
\end{aligned}
\qquad (30)
$$

where $[K_{p\min},\ K_{p\max}]$, $[K_{i\min},\ K_{i\max}]$ and $[K_{d\min},\ K_{d\max}]$ are the ranges of K_p, K_i and K_d, respectively.

6. Simulation results

We now separate the behaviours between finger and object into four cases, as illustrated in Figure 5. In all cases, the distal phalanx is always the last finger in contact with the object. Therefore, the process follows four steps: Firstly, the input torque of the ADAMS model is issued to move the finger; secondly, the virtual force sensors in the ADAMS model is generated during finger grasping; thirdly, the system will inspect how many phalanges in contact with the object and decide which case of finger behaviour will be used to determine the contact forces; and, finally, the proposed method will to start to calculate contact forces after contact between the distal phalanx and object.

In this paper, two simulations are used to apply the proposed method to determine the contact forces between the phalanges and the object. In the first simulation, the torque input is constant, while contact forces in each case are calculated by the proposal method based on inputs, such as rotating angles of phalanges and driving bars, the measured contact forces and motor torque input. The results are then compared with measured contact forces from the ADAMS model to prove the correctness of the proposed method. The second simulation is to apply the position and force control approaches in order to evaluate the convergence and stability of the system.

6.1 The first simulation results

In the first simulation, there are three input torques for each case: T_1=1.0[Nm], T_1=1.5[Nm] and T_1=2.0[Nm]. The contact forces of four cases are shown in Figures 13 to 24. In these figures, the measured contact forces (dash dot lines) are obtained from the force measurement functions in the ADAMS/View environment, while the calculated contact forces (solid lines) are computed by using the proposed method for determining the distributions of contact forces in Section 4.

As demonstrated by our simulation results, in case 1, three phalanges contact the object. From Figures 13 to 15, with three input torques, 1.0[Nm], 1.5[Nm] and 2.0[Nm], the calculated contact forces are very close to the three measured values. For instance, with the input torque T_1 =1.0[Nm], the calculated and measured contact forces F_1 and F_{m1} are 10.1289 [N] and 10.0779 [N] at proximal phalanx, F_2 and F_{m2} are 5.7138 [N] and 5.6525 [N] at medial phalanx, and F_3 and F_{m3} are 7.8316 [N] and 7.7661 [N] at distal phalanx, respectively. The closing between the calculated and measured contact forces proves that the proposed method can be used to determine the contact forces accurately. However, there are significant errors between the measured and calculated contact forces because of the effect of the mass of gripper elements and the frictions in the ADAMS model. Therefore, it can see that the three calculated and measured contact forces are also suitable with the input torques T_1=1.5[Nm] and T_1=2.0[Nm], even though the finger is a non-linear system.

In case 2, the proximal and distal phalanges make contact with the object, which means that there is no contact force between the medial phalanx and object. In turn, the measured contact force F_{m2} on the medial phalanx is zero, and the calculated force F_2 is also set to be zero, as illustrated in Figures 16 to 18. From these above figures, it can see that the calculated contact forces on the proximal and distal phalanges, F_1 (14.3496[N], 20.7475[N], 27.0532[N]) and F_3 (8.1763[N], 12.6521[N], 17.3404[N]), are still close to the measured values, F_{m1} (14.1518[N], 20.3435[N], 26.7318[N]) and F_{m3} (8.1505[N], 12.6104[N], 17.2194[N]). It can be seen that the proposed method still determines the contact forces precisely in the case of fewer-than-n phalanx grasping.

Figures 19 to 24 show the results of cases 3 and 4. Analyses of these two cases are similar to case 2.

Finally, as demonstrated in four cases, the simulation results show that the proposed method is very effective for determining the contact forces in the case of fewer phalanges touching the object in finger grasping.

6.2 The second simulation results

In the second simulation, the integrated control system, which combines the position and force control processes in finger grasping, is used. Firstly, the performance of the position control process is based on the desired angle position inputs until the distal phalanx touches the object, after which the system switches to the force control process. In the force control process, the contact force feedback is the calculated contact force on the distal phalanx, which is made using the proposed method. There are two desired contact forces on distal phalanx in four cases of gripper behaviour: F_{3d}=10[N] and F_{3d}=14[N].

As demonstrated by our second simulation results, in case 1, three phalanges contact the object. Figure 25 shows the desired and real angle position of the finger. It can be seen that the desired value is 1.4 [rad] while the real value comes up to 0.7 [rad] because the finger is prevented by the object. During the time from 0 to 0.65 [s], the real angle is close to the desired value, thereby proving that the position control process works well and is stable. Figures 26 and 27 show the calculated forces from CFD and the measured contact forces from the ADAMS model, as well as comparing with the desired contact forces. For instance, in Figure 26, the calculated force F_3 (dash line), after three oscillations, goes to the steady state and is close to the desired contact force, F_{3d}=10[N] (cyan line). It proves that the system is very stable and convergent, and its stability and convergence are also expressed, while the desired input F_{3d} changing from 10[N] to 14[N], as shown in Figure 27, F_3 is still close to the F_{3d}. Meanwhile, the three measured contact forces, F_{m1}, F_{m2} and F_{m3}, from the ADAMS model are still close to the three calculated contact forces, F_1, F_2 and F_3, in case 1 with F_{3d}=10[N] and F_{3d}=14[N], as illustrated in Figures 26 and 27. It shows that the proposed method is still precise in the control application, even though the finger is a non-linear system.

In case 2, the proximal and distal phalanges contact with the object, it means that there is no contact force between the medial phalanx and the object. The desired and real angle positions of the finger are shown in Figure 28. The real value comes up to 0.95 [rad] because the finger is prevented by the object. During the time from 0 to 1 [s], the real angle is close to the desired value, which proves that the position control process still works well and with stably. The calculated forces F_3 (dash line) still go to the steady state and are close to the desired contact force, F_{3d}=10[N] and F_{3d}=14[N] (cyan line), while the measured contact forces F_{m1} are also close to the calculated contact forces F_1, as shown in Figures 29 and 30. It proves that the system is still stable and convergent, and that the proposed method still determines the contact forces precisely in the case of fewer-than-n phalanx grasping.

Figures 30 to 36 show the results of cases 3 and 4. Analyses of these two cases are similar to the case 2.

In total, the second simulation results show that the system can perform stably, while the proposed method is very effective for estimating the contact forces as well as in control applications in the case of fewer phalanges touching the object in finger grasping, as demonstrated by four cases.
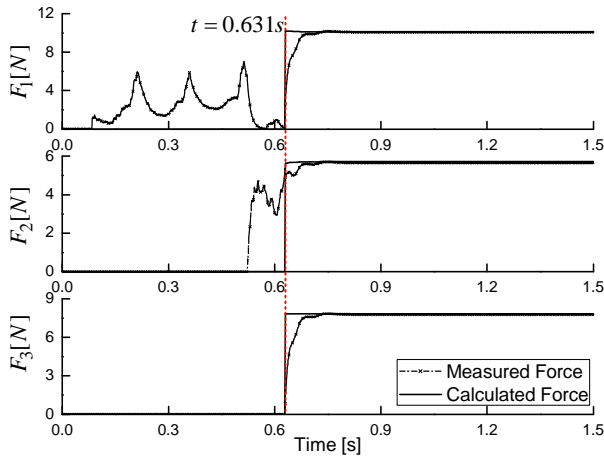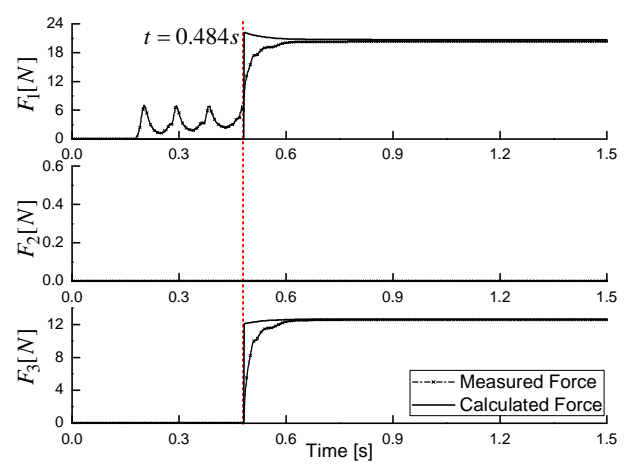
Figure 13. Contact forces with parameters $T_1=1.0[Nm]$, $k_1=0.037[m]$, $k_2=0.018[m]$ and $k_3=0.018[m]$ in case 1
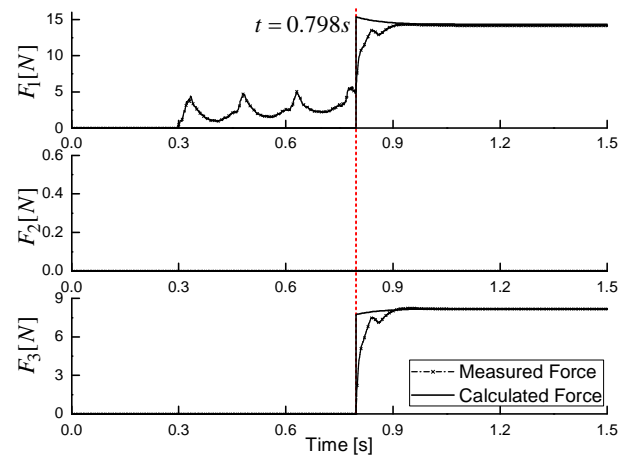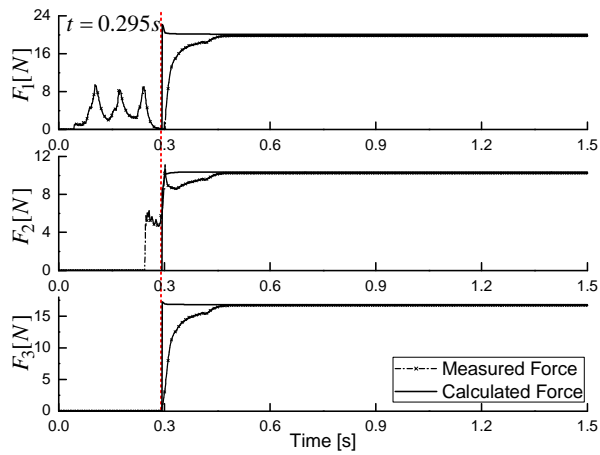

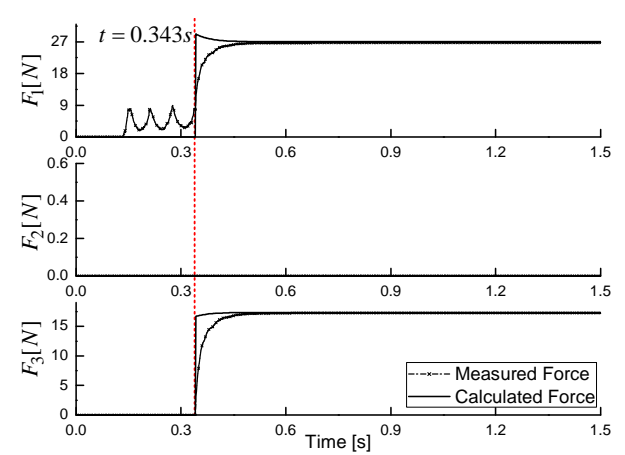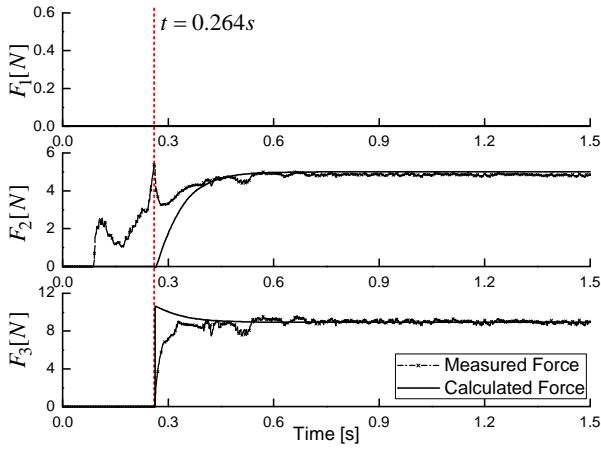**Figure 16.** Contact forces with parameters $T_1=1.0[Nm]$, $k_1=0.048[m]$ and $k_3=0.020[m]$ in case 2
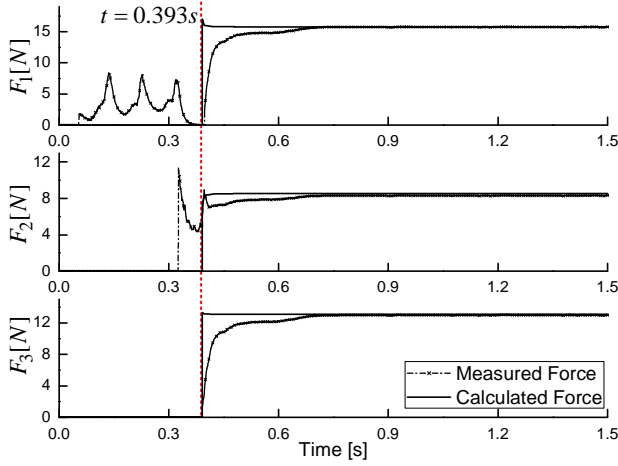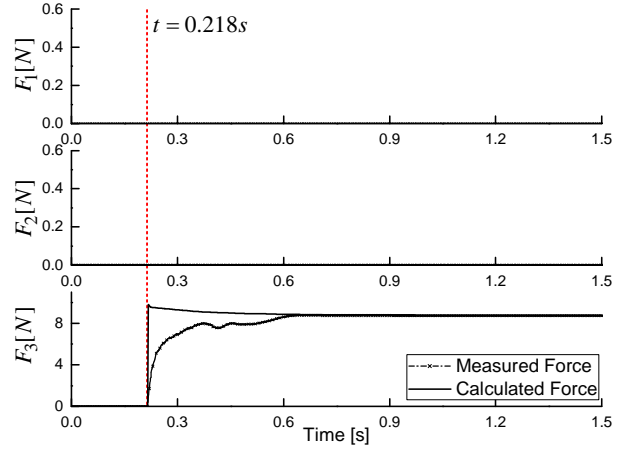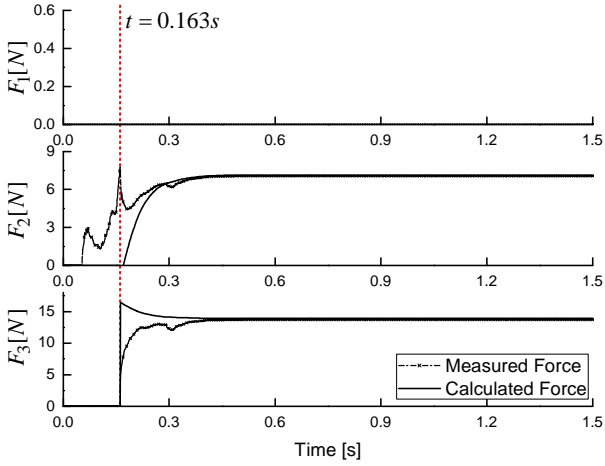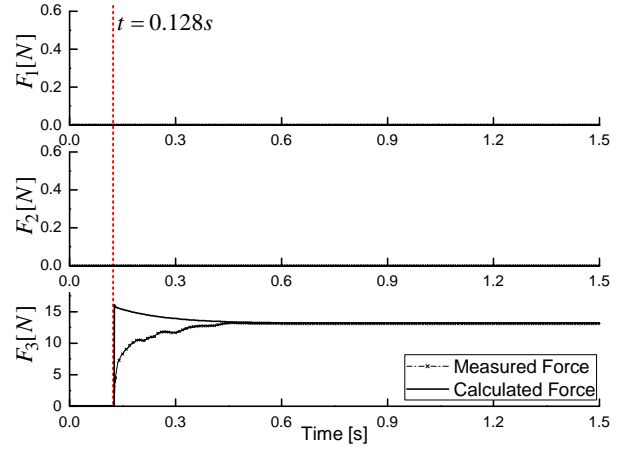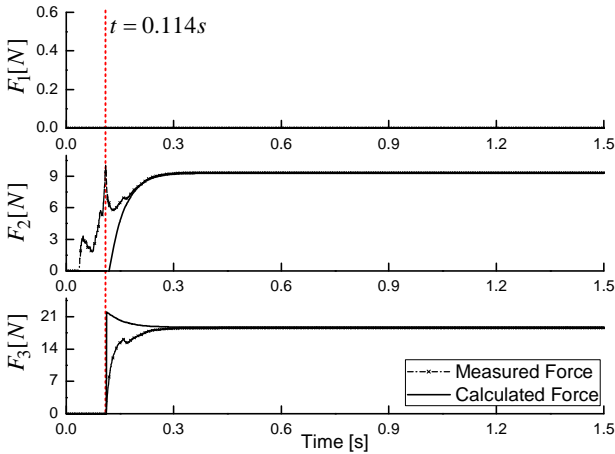

Figure 14. Contact forces with parameters $T_1=1.5[Nm]$, $k_1=0.037[m]$, $k_2=0.018[m]$ and $k_3=0.018[m]$ in case 1

Figure 17. Contact forces with parameters $T_1=1.5[Nm]$, $k_1=0.048[m]$ and $k_3=0.020[m]$ in case 2

Figure 15. Contact forces with parameters $T_1=2.0[Nm]$, $k_1=0.037[m]$, $k_2=0.018[m]$ and $k_3=0.018[m]$ in case 1

Figure 18. Contact forces with parameters $T_1=2.0[Nm]$, $k_1=0.048[m]$ and $k_3=0.020[m]$ in case 2

Figure 19. Contact forces with parameters $T_1=1.0[Nm]$, $k_2=0.023[m]$ and $k_3=0.017[m]$ in case 3

Figure 22. Contact forces with parameters $T_1=1.0[Nm]$ and $k_3=0.018[m]$ in case 4

Figure 20. Contact forces with parameters $T_1=1.5[Nm]$, $k_2=0.023[m]$ and $k_3=0.017[m]$ in case 3
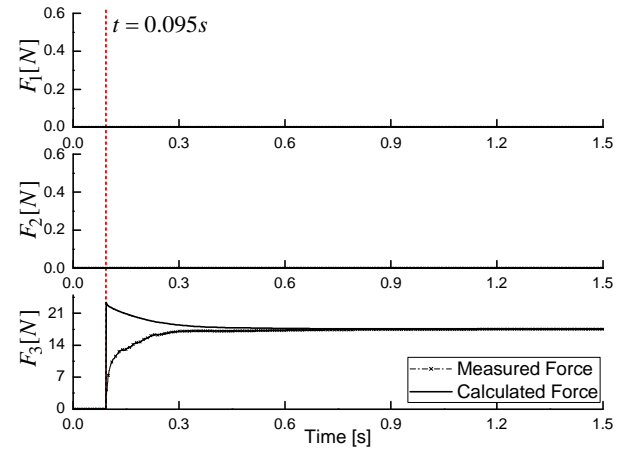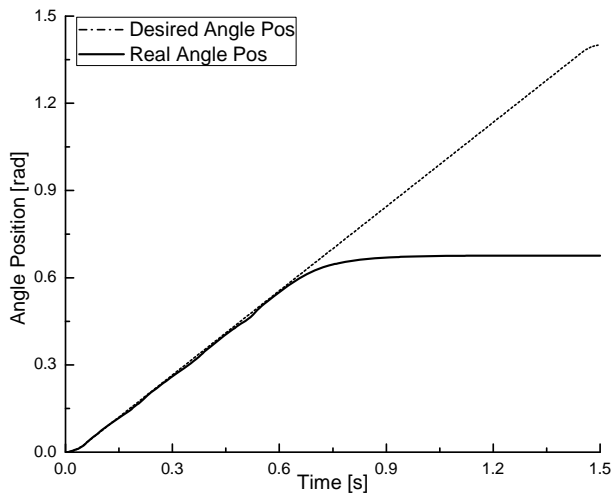

Figure 23. Contact forces with parameters $T_1=1.5[Nm]$ and $k_3=0.018[m]$ in case 4

Figure 21. Contact forces with parameters $T_1=2.0[Nm]$, $k_2=0.023[m]$ and $k_3=0.017[m]$ in case 3

Figure 24. Contact forces with parameters $T_1=2.0[Nm]$ and $k_3=0.018[m]$ in case 4

Figure 25. The desired and real angle positions of finger in case 1
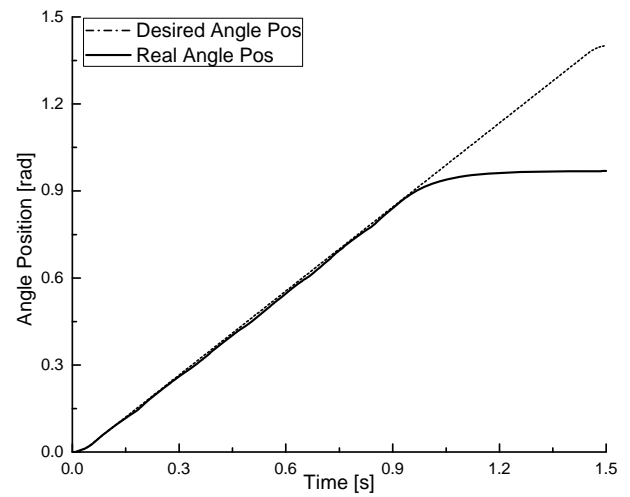
Figure 28. The desired and real angle positions of finger in case 2
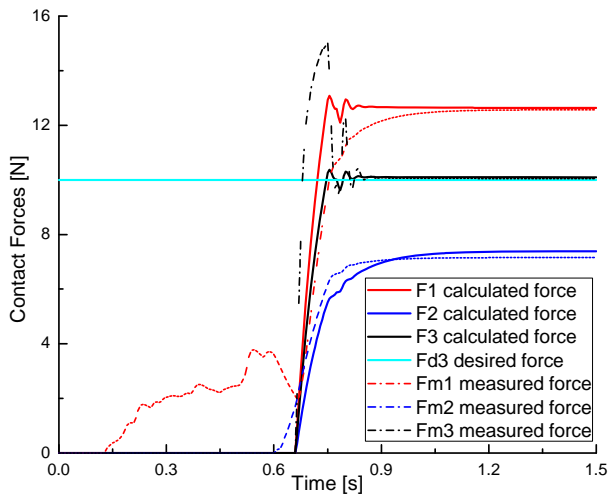

Figure 26. The calculated and measured contact forces of finger with the force feedback control in case 1, $F_{3d} = 10[N]$
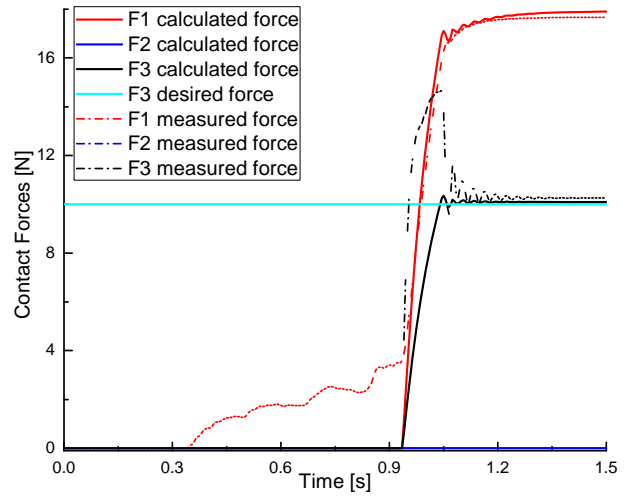

Figure 29. The calculated and measured contact forces of finger with the force feedback control in case 2, $F_{3d} = 10[N]$
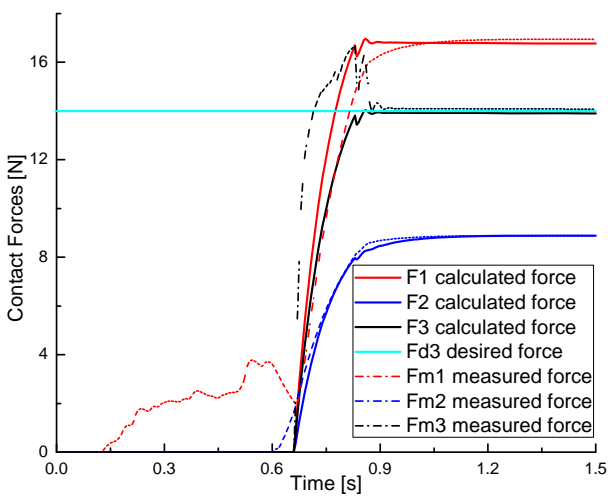

Figure 27. The calculated and measured contact forces of finger with the force feedback control in case 1, $F_{3d} = 14[N]$
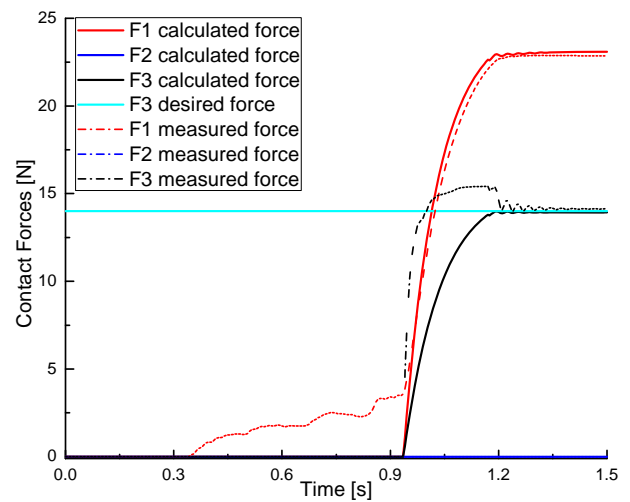

Figure 30. The calculated and measured contact forces of finger with the force feedback control in case 2, $F_{3d} = 14[N]$
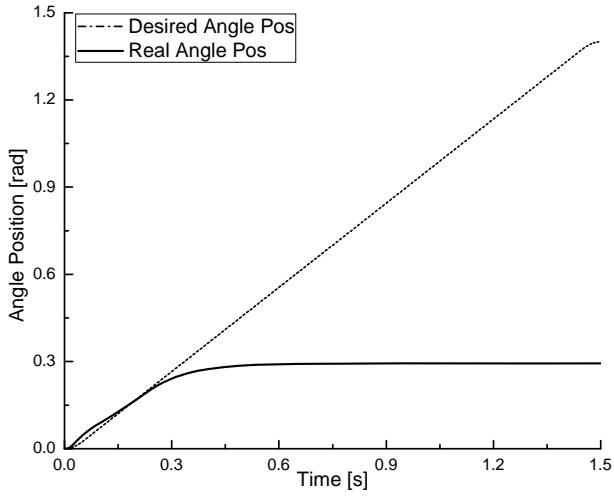
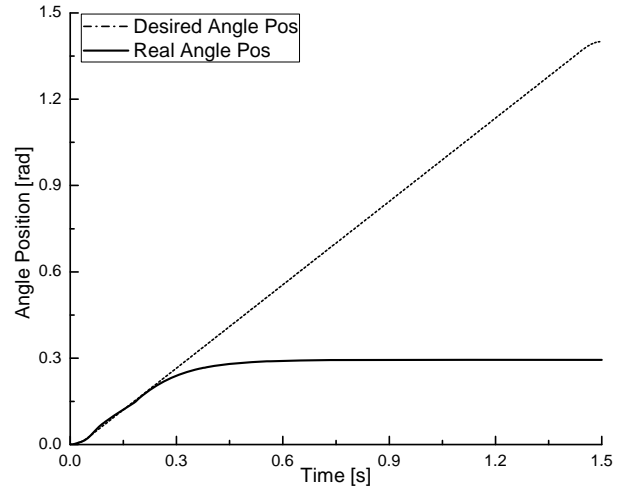**Figure 31.** The desired and real angle positions of finger in case 3

Figure 34. The desired and real angle positions of finger in case 4
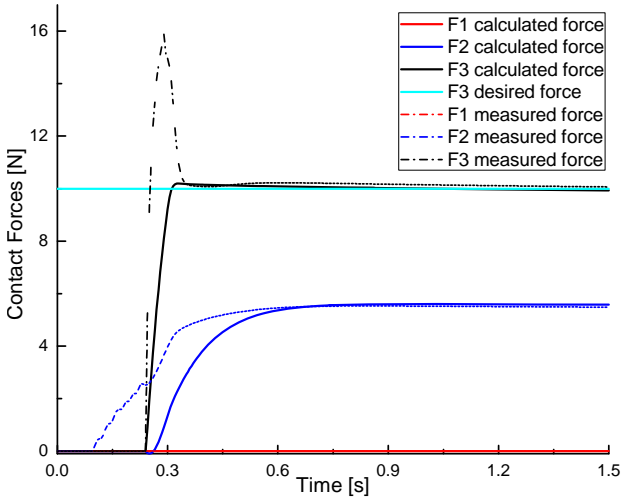

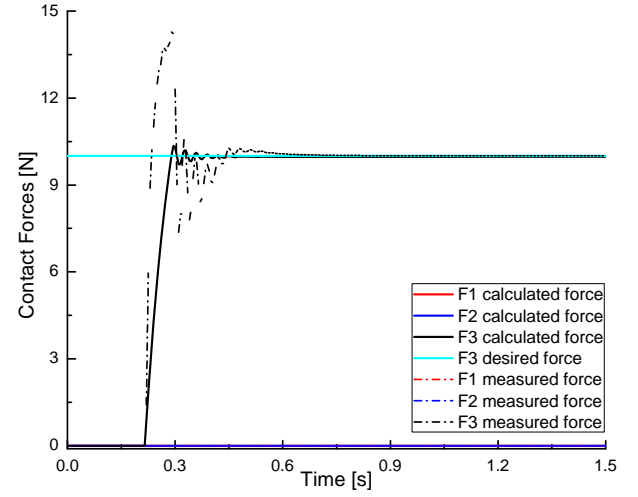**Figure 32.** The calculated and measured contact forces of finger with the force feedback control in case 3, $F_{3d} = 10[N]$

Figure 35. The calculated and measured contact forces of finger with the force feedback control in case 4, $F_{3d} = 10[N]$
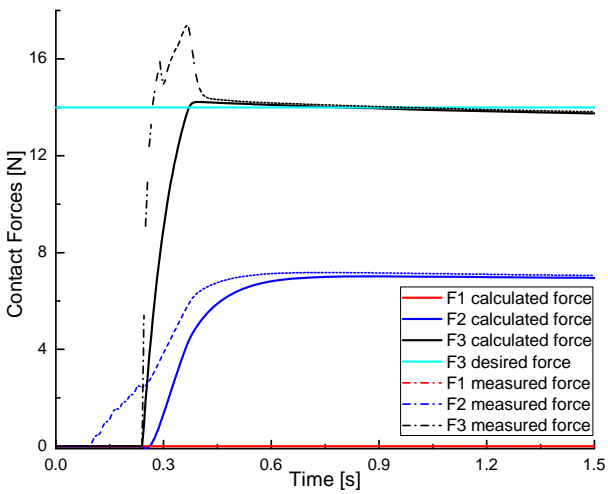

Figure 33. The calculated and measured contact forces of finger with the force feedback control in case 3, $F_{3d} = 14[N]$
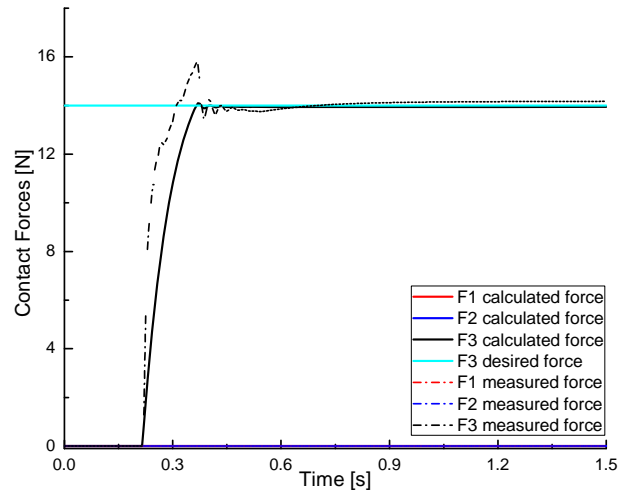

Figure 36. The calculated and measured contact forces of finger with the force feedback control in case 4, $F_{3d} = 14[N]$

7. Discussion

The introduction of two new matrices in [15] allows the system to calculate the contact forces on the phalanges through the input torque of the finger actuator in the case of full-phalanx grasping. Configurations of the finger leading to stable grasps are considered by using these two matrices. However, in order for a less-than-n phalanx grasp to be stable, every phalanx in contact with the object should have a strictly positive corresponding force. Actually, the contacts appear not only with all phalanges, but also with fewer-than-n phalanges in object grasping. The corresponding generated forces for phalanges not in contact with the object should be zero, since the latter forces can also be seen as the external forces needed to counter the actuation torque. Moreover, calculating contact forces in the case of fewer-than-n phalanges touching the object by using Equation (14) can be a problem because of the singularity of the J_T matrix. The proposed method in this paper, then, solves the above special case. A general mathematical analysis of the distributions of contact forces for the under-actuated finger was presented in the case of full-phalanx grasping, while taking into account cases of fewer-than-n phalanx grasping.

Lionel Birglen et al. believed that static analysis can help refine under-actuated finger designs in term of geometric parameters in order to achieve stable grasps and phalanx force distribution, avoiding weak last phalanges that cannot ensure sufficient force to secure the grasp [15]. Furthermore, with regard to the finger design process, the proposed method provides designers with a tool to select motor specifications (e.g., motor torque) and evaluate the object grasping forces, as well as provide the sensor-based contact force feedbacks for control strategies.

As mentioned in Section 5, the simulation technique based on the virtual prototype significantly reduces manufacturing cost and time compared to the traditional build-and-test approach. The virtual prototyping approach is an integrating software solution that consists of modelling a mechanical system, simulating and visualizing its 3D motion behaviour under real world operating conditions, as well as refining and optimizing the design through iterative design studies. The advantages of this simulation technique consist of conceiving a detailed model, which is used in a virtual experiment similar to a real scenario. Virtual measurements of parameters and components of the mechanical model can also be carried out conveniently. In light of the above reasons, authors have decided to choose the ADAM/View software to simulate the under-actuated finger. This includes real world operating conditions, such as material finger, friction parameters of joints, contact parameters (stiffness, force exponent, damping ratio and penetration depth) between phalanges and object. From the virtual prototyping process, the real system will be manufactured based on the simulation results.

The proposed method in this paper offers good simulation results in determining the contact forces and control application. The system is stable and convergent. Therefore, the proposed method can be applied in the real time experiment. Javier Felip et al. implemented and validated the robust grasp primitive for the BarrettHand gripper based on the sensor feedbacks from torque/torque and tactile sensors [19]. In order to control under-actuated hands, the MARS prototype finger's phalanges has been equipped with Force Sensing Resistors (FSR) to allow experimental testing of the added value of tactile sensing, as shown in Figure 1 [20]. In our gripper system, the potentiometers are installed at the phalanx joints to get the phalanx angles, while tactile sensors provide the contact positions between phalanges and object, while the torque sensors are also applied to measure the input torques. These sensors provide all the parameters needed to apply the proposed method to estimate the contact forces, which will be used to force feedbacks in the finger control strategies. In turn, this provides a low-cost, high performance and easy-to-use operation system.

Given the nonlinear system, intelligent control approaches have been developed, such as the sliding mode controller (SMC) or the Fuzzy Logic Controller (FLC). In gripper control strategy, tactile sensing is of the utmost importance. By using these sensors, one can design a closed-loop force controller and, for example, detect whether the grasping forces are on the edge of vanishing and, in the process, resume the grasping actuation. Moreover, the robustness in grasp task is not only achieved by designing sensor-based controllers, but also by combining several controllers with different optimisation goals. This will be done in real time experimentation in future studies.

8. Conclusions

This paper presents a mathematical analysis to determine the distribution of contact forces for the under-actuated finger in general grasping cases of an under-actuated robotic hand. Due to the importance of the contact forces, the proposed method for static analysis of the distributions of the contact forces focuses on the n-DOF under-actuated finger. The simulation results, with the 3-DOF under-actuated finger from the ADAMS model, show the effectiveness of the mathematical analysis method, as well as comparing the measured results with, especially, the stability and convergence in control application. The system can find magnitudes of the contact forces at the contact positions between the finger phalanges with the object.

9. Acknowledgements

10. References

[1] Hirose, S. and Umetani, Y. (1978) The development of soft gripper for the versatile robot hand. Mechanism and Machine Theory: 13, 351-358.

[2] Birglen, L. and Gosselin, C. (2004) Optimal Design of 2-Phalanx Under-actuated Fingers. Proceedings of the International Conference on Intelligent Manipulation and Grasp: 110–116.

[3] Jacobsen, S.C., Iversen, E.K., Knutti, D.F., Johnson, R.T. and Biggers, K.B. (1986) Design of the UTAH/MIT dextrous hand. IEEE International Conference on Robotics and Automation: 1520–1532.

[4] Salisbury, J.K. and Craig, J. J. (1982) Articulated hands: Force control and kinematic issues. International Journal of Robotics Research: 1, 4–17.

[5] Bekey, G.A., Tomovic, R. and Zeljkovic, I. (1999) Control Architecture for the Belgrade/USC Hand in Dextrous Robot Hands. Springer-Verlag, New York.

[6] Butterfass, J., Grebenstein, M., Liu H. and Hirzinger G. (2001) DLR-hand II: Next generation of a dextrous robot hand. IEEE International Conference on Robotics and Automation: 1, 109–114.

[7] Corrales, J.A., Jara, C.A. and Torres, F. (2010) Modelling and simulation of a Multi-fingered Robotic Hand for Grasping Tasks. International Conference on Control, Automation, Robotics and Vision: 1577-1582.

[8] Rizk, R., Krut, E. and Dombre, E. (2007) Grasp-stability analysis of a two-phalanx isotropic underactuated finger. Proceedings of the International Conference on Intelligent Robots: 3289-3294.

[9] Dandash, G., Rizk, R., Krut, E. and Dombre, E. (2011) A pseudo-isotropic three-phalanx underactuated finger. World Congress in Mechanism and Machine Science: 1-8.

[10] Peer, A., Einenkel, S. and Buss, M. (2008) Multi-fingered telemanipulation - mapping of a human hand to a three finger gripper. IEEE International Symposium on Robot and Human Interactive Communication: 465 - 470.

[11] Laliberté, T. and Gosselin, C.M. (1998) Simulation and design of underactuated mechanical hands. Mechanism and Machine Theory: 33, 39–57.

[12] Laliberté, T., Birglen, L. and Gosselin, C. (2002) Underactuation in robotic grasping hands. Journal of Machine Intelligence and Robotic Control: 4, 1-11.

[13] Petković, D., Pavlović, N.D., Žarko Ćojbašić, Z. and Pavlović, N.T. (2013) Adaptive neuro fuzzy estimation of underactuated robotic gripper contact forces. Expert Systems with Applications: 40, 281–286.

[14] Birglen, L. and Gosselin, C.M. (2006) Force analysis of connected differential mechanisms: Application to grasping. International Journal of Robotics Research: 25, 1033-1046.

[15] Birglen, L. and Gosselin, C.M. (2004) Kinetostatic analysis of underactuated fingers. IEEE Transactions on Robotics and Automation: 20, 211-221.

[16] Ceccarelli, M., Tavolieri, C. and Lu, Z. (2006) Design Considerations for Underactuated Grasp with a one D.O.F. Anthropomorphic Finger Mechanism. International Conference on Intelligent Robots and Systems: 1611 – 1616.

[17] Wu, L., Carbone, G. and Ceccarelli, M. (2009) Designing An Underactuated Mechanism for a 1 Active Dof Finger Operation. Mechanism and Machine Theory: 44, 336-348.

[18] Ceccarellia, M. and Zottolaa, M. (2015) Design and simulation of an underactuated finger mechanism for LARM Hand. Robotica: Available on CJO 2015 doi:10.1017/S0263574715000648, 15 pages.

[19] Felip, J. and Morales, A. (2009) Robust sensor-based grasp primitive for a three-finger robot hand. IEEE / RSJ International Conference on Intelligent Robots and Systems: 1811 - 1816.

[20] Birglen, L., Gosselin, C.M. and Birglen, L. (2005) Fuzzy Enhanced Control of an Underactuated Finger Using Tactile and Position Sensors. IEEE International Conference on Robotics and Automation: 2320 - 2325.

[21] Norton, R.L. (1992) Design of Machinery. New York: McGraw-Hill, Inc.

[22] McCarthy, J.M. (2000) Geometric Design of Linkages. New York: Springer-Verlag.

[23] Xuan Vinh Ha, Cheolkeun Ha and Jewon Lee, (2013) Fuzzy Vector Field Orientation Feedback Control-Based Slip Compensation for Trajectory Tracking Control of a Four Track Wheel Skid-Steered Mobile Robot. International Journal of Advanced Robotic Systems: 10, pages 15.